Int. J. Electrochem. Sci., 10 **(2015)** 1169 - 1185

International Journal of
ELECTROCHEMICAL
SCIENCE
www.electrochemsci.org

Electrochemical Corrosion Behavior and Prediction of Corrosion Rate for Low Alloy Steel after Tempering Treatment

Hongwei Wang[1,*], *Chi Yu*[2], *Suxin Wang*[1], *Jing Gao*[1]

[1] School of Information Science & Engineering, Northeastern University, Shenyang 110819, China;
[2] School of Materials & Metallurgy, Northeastern University, Shenyang 110819, China.
[*]E-mail: wanghw0819@163.com

Received: 3 November 2014 / *Accepted:* 7 December 2014 / *Published:* 16 December 2014

The electrochemical corrosion behavior and prediction of corrosion rate for low alloy steel after tempering treatment in acid 3.5wt.% NaCl solution is investigated. First, the effects of tempering temperature on microstructures are analyzed by optical microscope (OM) and scanning electron microscopy(SEM). Then, the corrosion rate of alloy steel is calculated by accelerated corrosion tests, it indicates superior corrosion resistance. The polarization curve and electrochemical impedance spectroscopy (EIS) are applied to research the corrosion process. The proper time constants are chosen for equivalent circuit to fit experimental results. Finally, the results of EIS are in agreement with accelerated corrosion and potentiodynamic polarization measurements by relating to known physical parameters. Finally, the prediction model of corrosion rate is established by using grey system theory, simulations result shows that the obtained mathematical model is feasible, which can be well used to forecast corrosion rate for the low alloy steel .

Keywords: low alloy steel; tempering treatment; electrochemical corrosion behavior; corrosion rate; prediction model

1. INTRODUCTION

The low alloy steel is mainly used in various environments, such as the atmosphere, marine and soil. So it not only requires good mechanical properties, but also has superior corrosion resistance. Recently, it has been found that low alloy steel after heat treatment exhibits well mechanical properties, with high tensile strength and good ductility. Many researchers have focused significant attention, obtained some results [1-3]. In practical applications, these alloys are possibly exposed to the special corrosion environment. A few papers have been devoted to the corrosion behavior of low alloy

steel [4-6]. Therefore, the corrosion problem of low alloy steel has very important research significance.

Now, word-wide there is increasing attention being given to reliable methods for corrosion problem. Weigh loss measurement is currently the most direct and reliable method but time consuming and information limited, so the corrosion resistance has been investigated by simulated and accelerated corrosion tests [7]. In addition, electrochemical measurement is a powerful tool for researching corrosion process, has obtained many good results by equivalent circuit method [8-11]. But few studies have been reported in the literature concerning the corrosion behavior of low alloy steel after tempering treatment under strong acid solution [12-13].

Currently, the grey system theory has a wide variety of applications [14-15]. Grey model GM (1, 1) is the simplest mathematical model to describe a grey system. The method can meet the request of prediction due to its advatages of little original data needed and high precision. The corrosion rate is varied with increasing the immersion time, establishing an effective mathematical model is very important. GM(1,1) method is very suit to solve the problem .

In this paper, corrosion behavior of low alloy steel after tempering is investigated. First, the effects of tempering temperature on microstructures are analyzed by optical microscope (OM) and scanning electron microscopy (SEM). Then, the accelerated corrosion tests are used to calculate corrosion rate. The polarization curve and electrochemical impedance spectroscopy (EIS) are obtained to analyze the corrosion behavior, and using Tafel fitting and equivalent circuit method, respectively. Finally, the mathematical model is established using GM (1, 1) method, which can predict corrosion rate. Simulations result indicates the obtained mathematical model is feasible.

2. EXPERIMENTAL MATERIAL AND PROCEDURES

2.1 Materials

The chemical composition of low alloy steel is listed in Table 1.

Table 1. Chemical compositions of low alloy steel (mass fraction, wt.%)

C	Si	Mn	P	S	Cu	Ni	Nb	Al	Ti	Ca	Mo	Fe
0.053	0.20	1.10	0.008	0.002	0.06	0.15	0.051	0.007	0.015	0.0015	0.16	Others

The study steel is heated at 950 ^{o}C for 60min and water-quenching. The samples are obtained after tempering at different temperatures (350 ^{o}C, 550 ^{o}C and 650 ^{o}C), denoted as T350, T550 and T650, respectively. The microstructures are observed by OM and SEM.

2.2 Accelerated corrosion tests

The samples are cut into 70 mm×30 mm×5.5 mm. Prior to testing, the specimens are ground

with a series of SiC waterproof abrasive papers (100, 600, 800, 1200 and 1500), washed with acetone and ethanol ultrasonic, and then dried by air, weighted using BS224S electronic balance weighing scales with a precision of 0.1mg, recorded as W_b. The corrosion medium is 3.5 wt.% NaCl solution, the pH value is adjusted to 3 with hydrochloric acid solution. After immersion, the specimens are removed, carefully cleaning with acetone and ethanol, dried at room temperature, and then weighted once every 24 hours, the temperature of test solution remains at 30 ^{o}C. The last weighing mass is denoted as W_a, so the weightlessness is $\Delta W = W_b - W_a$. In order to reduce the error, experiments are performed using three parallel samples and the mean value is calculated.

2.3 Electrochemical measurements

The specimens with an exposed surface of 1cm^2 are used for electrochemical experiment, the other sides are coated with an insulating material. Prior to testing, the samples are ground with a series of SiC waterproof abrasive papers (100, 600, 800, 1200 and 1500), washed with acetone and ethanol ultrasonic, and then dried by air. In electrochemical experiment, all the conditions are the same as weight loss test. The electrochemical measurement is conducted on the samples with different immersion time in 3.5 wt.% NaCl.

The electrochemical measurements are performed by a PATSTAT2273 electrochemical workstation with PowerSuite software. A conventional three-electrode cell is used. It contains the platinum electrode as the auxiliary electrode, the saturated calomel electrode (SCE) as the reference electrode, which is connected to the NaCl acid solution via a Luggin capillary and a salt bridge, and the sample as the working electrode. All polarization curves are recorded potentiodynamic with a scan rate of 1mV/s and the potential range from 100 mV to -100mV vs corrosion potential, and a CorrWiew software is used to analyze the polarization curves. The EIS experiments are measured in open circuit voltage with amplitude of 8 mV and a frequency range of 10^5-10^{-1} Hz, and Zsimpwin software is used to analyze the EIS results by equivalent circuit method.

3. RESULTS AND DISCUSSION

3.1 Microstructures

Figure 1 shows the microstructures of low alloy steel at different tempering temperatures. As indicated in Figure 1(a, b) for tempering at 350 ^{o}C, the microstructure is bainitic ferrite (BF) and granular bainite (GB). The grain size is uniformity, the strip M/A constituent exists at the grain boundary, and the interior sub-lath of some GB begins to merge and its boundary disappeared. After being tempered at 550 ^{o}C, the microstructure is still BF+GB in Figure 1(c, d). Inner substructure of GB disappears, M/A island turns into tiny and spotty particles because of gradual decomposition. As shown in Figure 1(e, f), the microstructure is made of granular bainite (GB) and quasi-polygonal ferrite (QF) when tempering at 650 ^{o}C, the M/A island constituent on grain boundary is decomposed, the grains of QF have grown up through grain boundary.

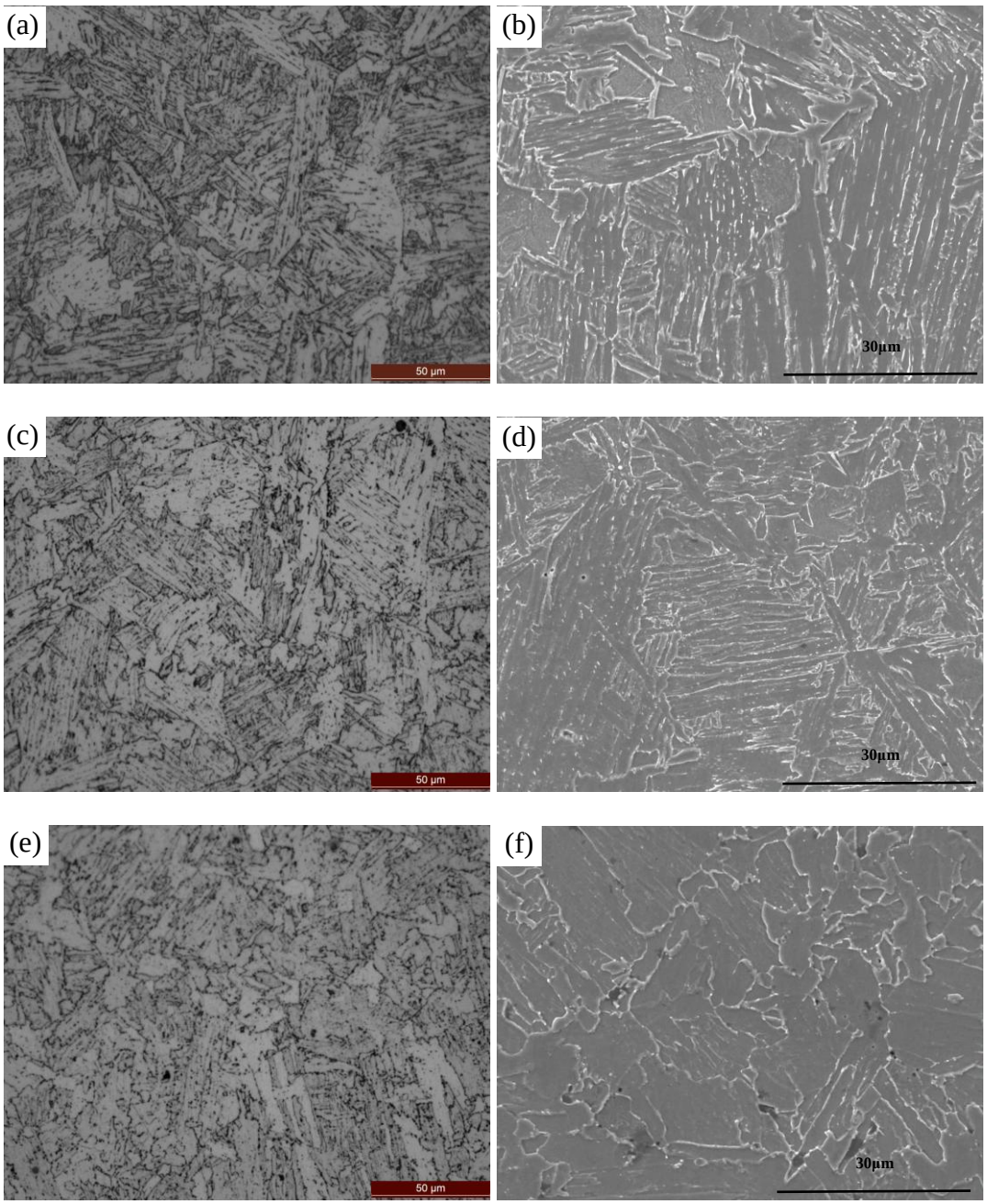

Figure 1. OM images and SEM images of low alloy steel at different tempering temperatures (OM: (a) 350 °C (c) 550 °C (e) 650 °C SEM: (b) 350 °C (d) 550 °C (f) 650 °C)

3.2 Accelerated corrosion tests

The corrosion rate of experimental steel in acid 3.5% NaCl solution is studied. The corrosion rate v is calculated according to the following equation [16].

$$v = \frac{8.76 \times 10^4 \times \Delta W}{S \times t \times \rho} \qquad (1)$$

where v is the corrosion rate, mm/a, ΔW is the weight loss, g, S is the total area of the sample, cm^2, t is the immersion time, h, and ρ is the density of the sample, g/cm^3.

The average corrosion rate calculated by equation (1) is shown in Table 2. As can be seen from the table 2, the corrosion resistance performance is good, the corrosion rates are between 0.36 ~ 0.71 mm/a. Among them, the corrosion resistance of T650 which contains more fine and homogeneous GB and QF microstructures is the best.

Table 2. Corrosion rate of low alloy steel

samples	T350	T550	T650
v (mm/a)	0.7055	0.5203	0.3624

The weight loss as a function of time is shown in Figure 2. We can see that the corrosion rate is also varied for three types of corrosion resistant steel under different immersion time. After immersing six days, the corrosion rates tend to be more stable. Among these steels, T650 keeps less weight loss, which shows the steel has superior corrosion resistance. All of these studies suggest that the microstructure of the corrosion resistant steel has significant effect on the corrosion rate.

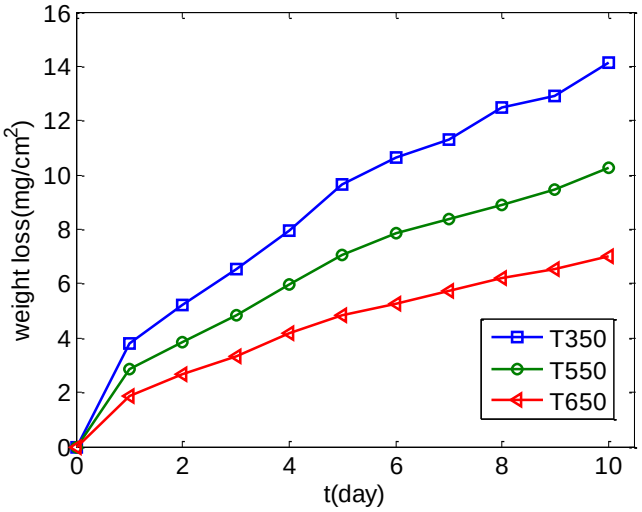

Figure 2. The weight loss of low alloy steel at different tempering temperature

The conversion of gravimetric parameters into electrochemical ones is made by means of Faraday's law [17].

$$i_{corr} = \frac{nF\Delta W}{MTS} \qquad (2)$$

where i_{corr} is corrosion current density, A/ cm^2, n is valence, F is Faraday's constant (96500 coulombs), ΔW is weight loss due to corrosion, g , M is molecular weight of metal, g/mol, T is the immersion time, s, S is the total area of the sample, cm^2. Figure 3 shows the variation of corrosion current density with increasing immersion time. It is seen that there is a period (about 6 days) during which there is initially a very high corrosion rate followed by a steady decline.

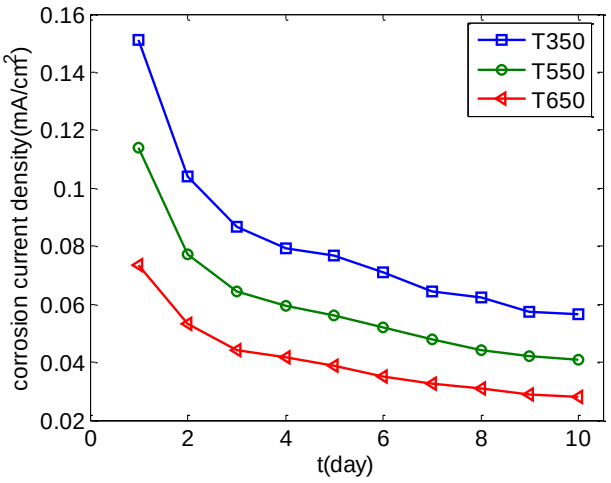

Figure 3. The corrosion current density of low alloy steel at different tempering temperature

3.3 Polarization Behaviors

The polarization curves of experimental steel are indicated in Figure 4. It can be seen that the anodic current density increases continuously with increasing potential, which indicate that all samples show active dissolution behaviors. Typical active dissolution behavior could be established on both curves. The anodic and cathodic branches show Tafel behavior. So Tafel extrapolation can be applied to calculate the corrosion kinetics parameters. The corresponding anodic potential (b_a), cathodic potential (b_c), corrosion potential (E_{corr}), and corrosion current density (I_{corr}) are given in Table 3. All these polarization curves have similar shapes in anodic and cathodic branches. The anodic and cathodic Tafel constants do not obviously change for samples, which show that the similar mechanism for corrosion reaction. It is found that the corrosion current density (I_{corr}) decrease with increasing of tempering temperature, which shows that the corrosion resistance is becoming better and better. The high corrosion current density represents big corrosion rate, it will be more prone to corrosion, and vice versa [13]. Visual observation after potentiodynamic polarization curves, we can clearly see that the electrode surface is severely corroded and presents black and much uneven.

The variation of corrosion current density with increasing immersion time is shown in Figure 5. The corrosion current density of T650 steel is smaller than other steels, which shows the well corrosion resistance. The corrosion current densities obtained by corrosion mass loss and potentiodynamic polarization method are shown in Figure 3 and Figure 5, respectively. It is indicates that the corrosion current densities are correlated with each other. With increase the immersion time, the corrosion rates tend to be more stable. It should point out that there exists some different about current densities between the accelerated corrosion and potentiodynamic polarization tests for the same samples because the measurement from the polarization curves is not steady. Finally, the obtained corrosion current density by the polarization curves measurements is consistent with those obtained by weight loss tests.

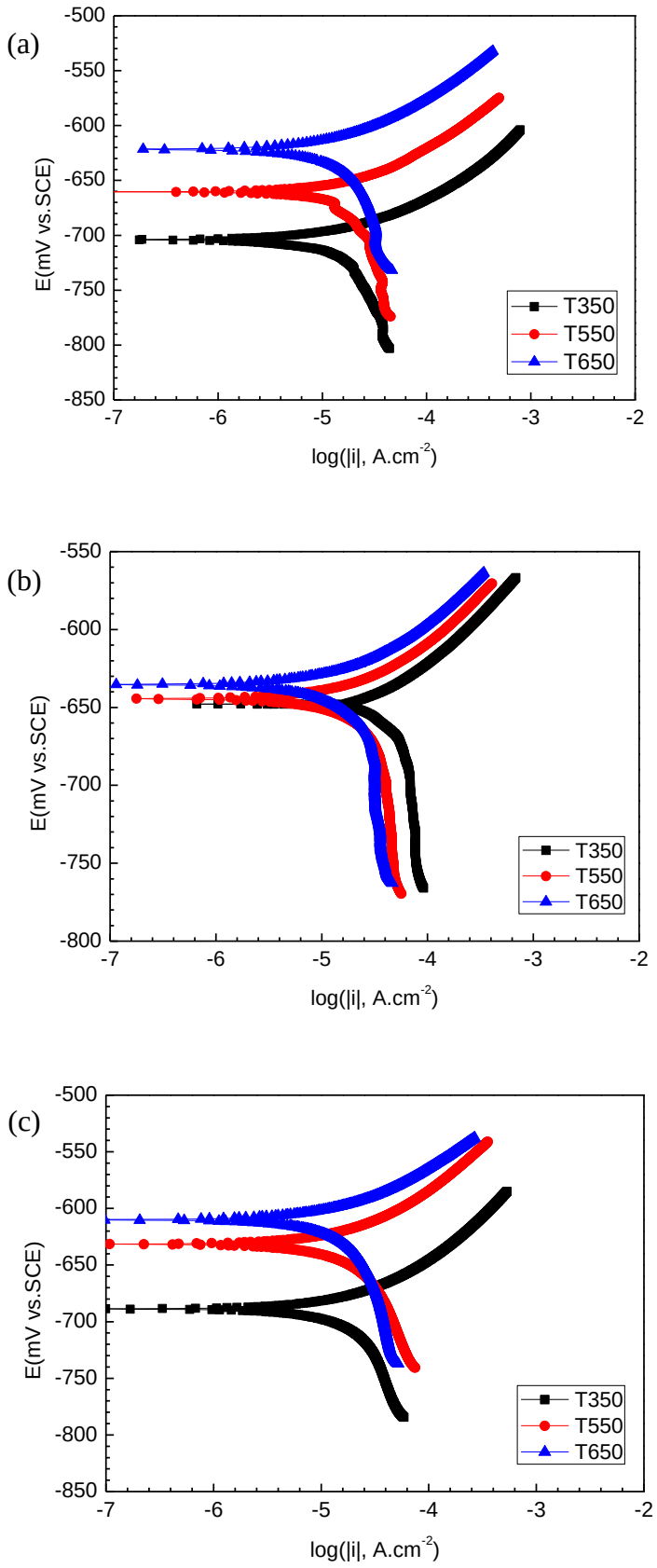

Figure 4. Potentiodynamic polarization curves of low alloy steel (a) bare steel (b) after 5 days immersion test (c) after 10 days immersion test

Table 3. Electrochemical parameters of polarization curves

Times	sample	b_a (mV/dec)	b_c (mV/dec)	E_{corr}(mV)	I_{corr}(10^{-2}mA/cm^2)
0day	T350	72	-191	-705	3.596
	T550	60	-129	-663	3.153
	T650	68	-162	-632	1.429
5days	T350	70	-178	-648	7.386
	T550	77	-184	-645	5.103
	T650	76	-199	-635	3.821
10days	T350	80	-96	-689	5.038
	T550	84	-152	-632	3.728
	T650	70	-104	-610	2.648

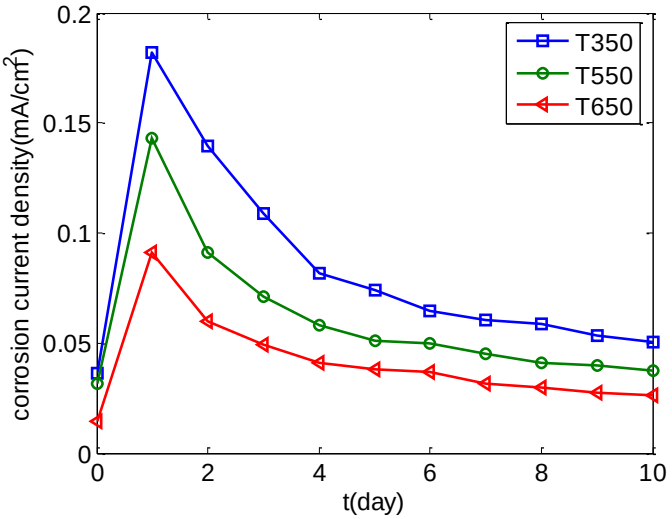

Figure 5. The corrosion current density of low alloy steel for polarization curves at different tempering temperature

3.5 Electrochemical impedance spectroscopy (EIS)

Figure 6 shows the typical Nyquist plots for bare steel samples, we can see that each spectrum includes an incomplete semicircle, the semicircle diameters of T650 is larger than samples T350 and T550, which indicate that the corrosion resistance of T650 is higher than other steels.

Bode diagrams are shown in Figure 7. It is seen that the impedance modulus will gradually bigger with the increase of tempering temperature. The impedance modulus of T650 steel is biggest, and the smallest one is T350 in the low frequency range. As shown in Figure 7(b), the broad-phase angle peak for the experimental steel can show at least two time constants. So the electrochemical behavior can be simulated by a simple equivalent circuit in Figure 8.

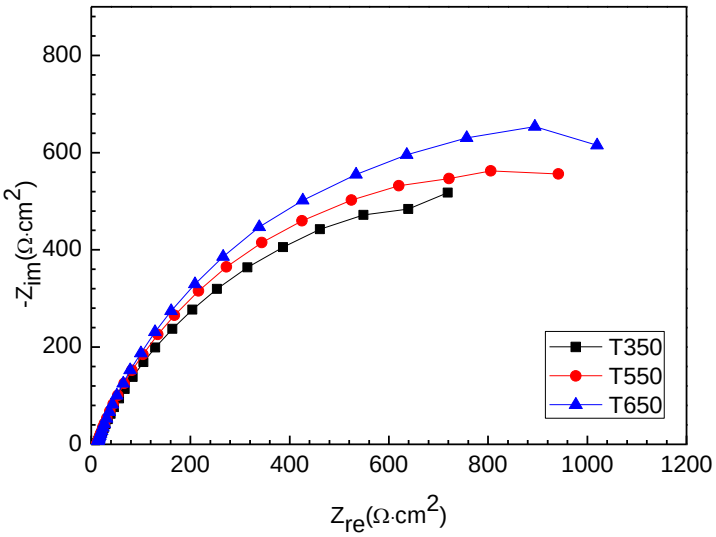

Figure 6. Nyquist plots for bare steel samples in 3.5 wt.% NaCl acid solution

Rs represents the electrolyte resistance, which is resistance of the solution between the work electrode and Luggin capillary. R_f is the resistance of corrosion product film. CPE is the constant phase element with an impedance given by $Z= \frac{1}{Y_0 (j\omega)^n}$, where Y_0 is a general admittance function equal to the capacitance C, j is the complex operator with $j=(-1)^{1/2}$, $\omega=2\pi f$ is the angular frequency, n is a power, which is an adjustable parameter that lies between 0 and 1. R_{ct} is the charge transfer resistance, which is used to represent the difficulty of the electrochemical reaction. The dates are obtained from the equivalent circuits, which are listed in Table 4.

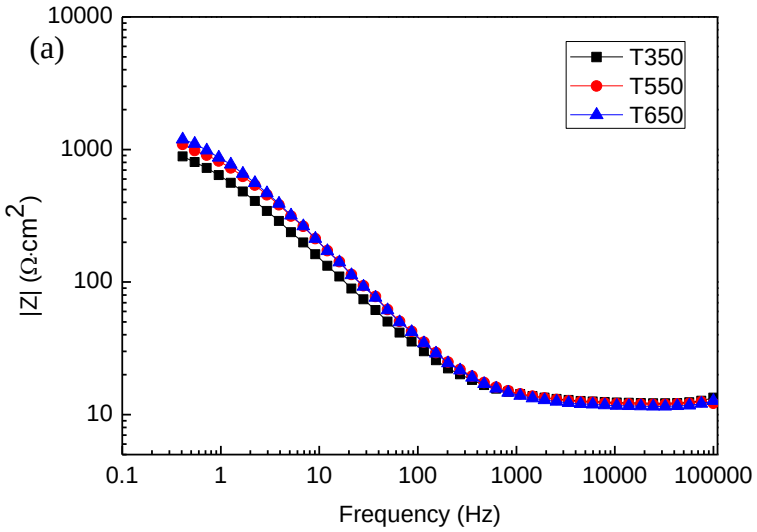

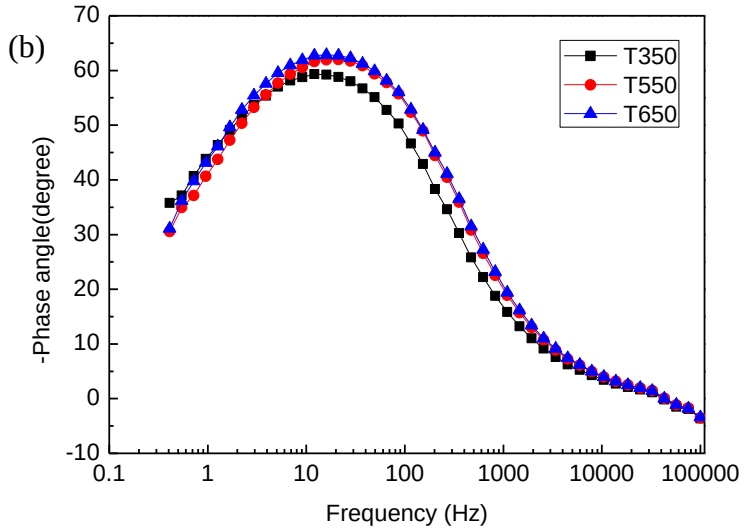

Figure 7. Bode diagrams of the bare steel samples in 3.5 wt.% NaCl acid solution (a) The amplitude-frequency characteristic curve (b) The phase-frequency characteristic curve

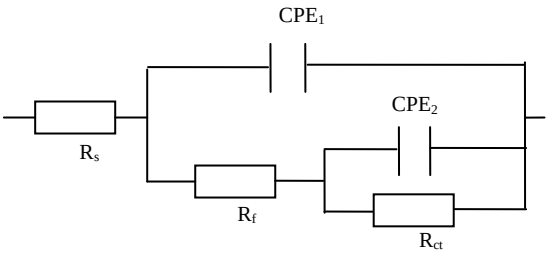

Figure 8. Equivalent circuits for low alloy steel

Table 4. Parameters of equivalent circuit

sample	R_s ($\Omega \cdot cm^2$)	Y_{01}(S-sec^n/cm^2)	n_1	R_f ($\Omega \cdot cm^2$)	Y_{02}(S-sec^n/cm^2)	n_2	R_{ct} ($\Omega \cdot cm^2$)
T350	12.25	0.0002645	0.7728	1186	0.001521	0.712	647
T550	11.97	0.0001792	0.7971	1297	0.002321	0.6725	1245
T650	11.60	0.0001809	0.7973	1549	0.001694	0.6728	2076

In order to clarify the corrosion process, the typical Nyquist plots and Bode diagrams of the experimental steel after 5 days and 10days immersion tests are displayed in Figure 9 and Figure 10, respectively. As a whole, the impedance modulus will gradually increase with the increase of tempering temperature. It is seen that the impedance modulus of T650 is biggest, which show that corrosion resistance of T650 steel are better than other steels. The curve of the experimental steel consists of a deformed semicircle with two time constants. The equivalent circuit mode is the same as that shown in Figure 8. The dates are obtained from the equivalent circuits, which are listed in Table 5.

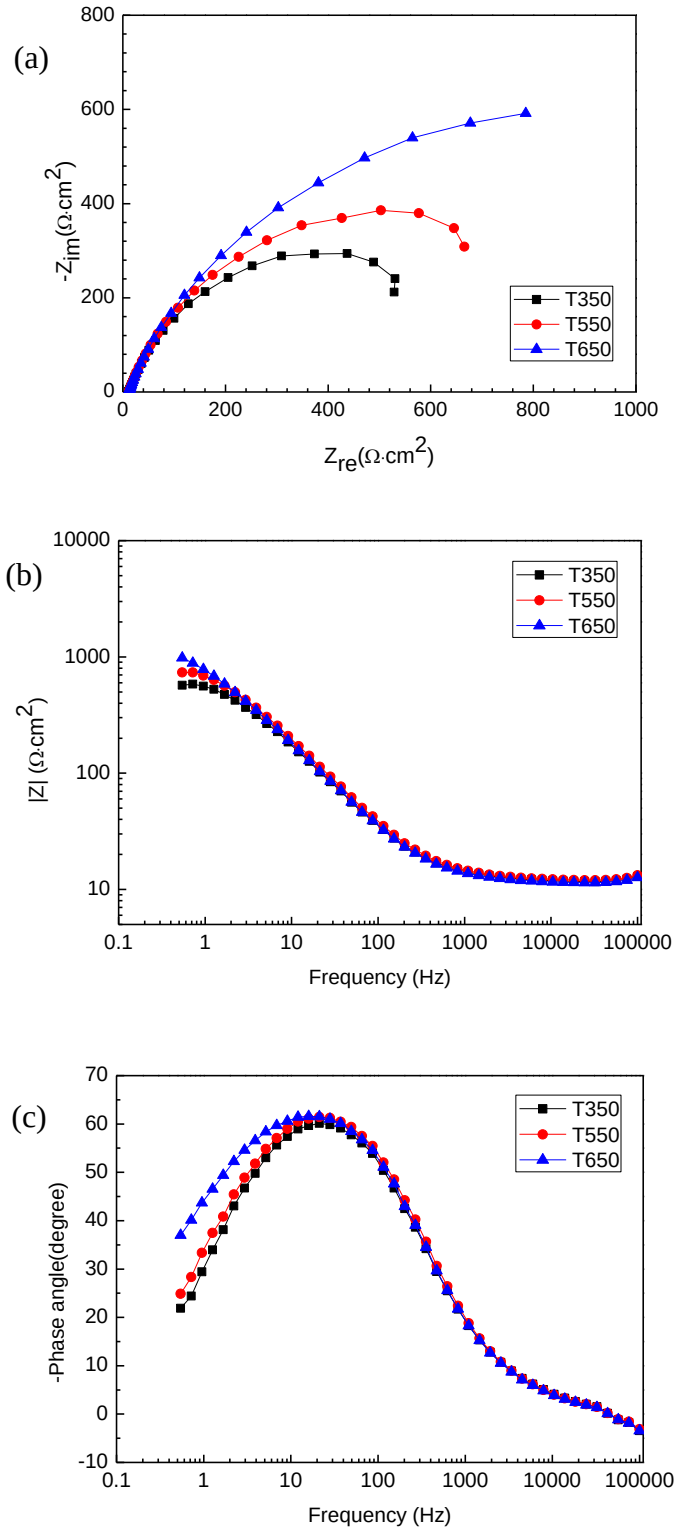

Figure 9. Nyquist plots and Bode diagrams of the low alloy steel after 5 days immersion test in 3.5 wt.% NaCl acid solution (a) Nyquist plots (b) The amplitude-frequency characteristic curve (c) The phase-frequency characteristic curve

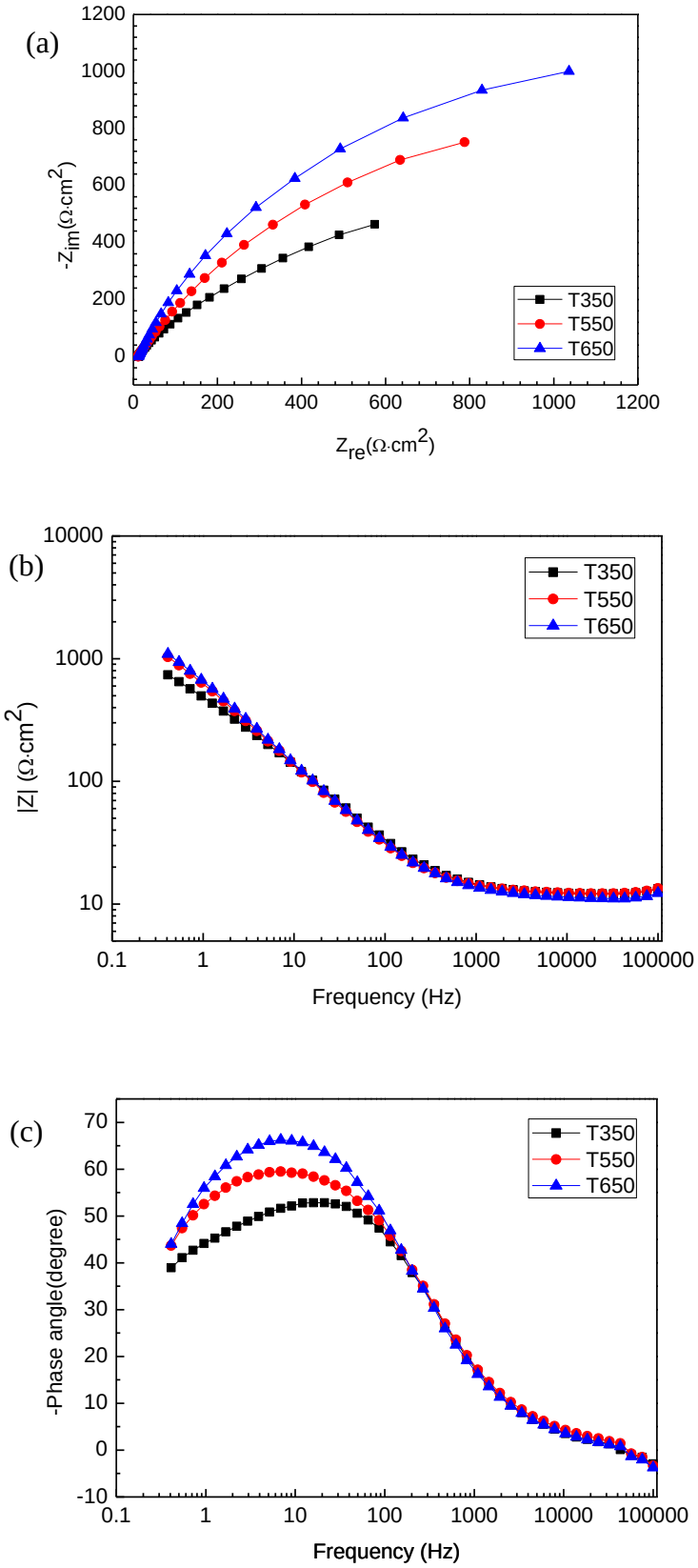

Figure 10. Nyquist plots and Bode diagrams of the low alloy steel after 10 days immersion test in 3.5 wt.% NaCl acid solution (a) Nyquist plots (b) The amplitude-frequency characteristic curve (c) The phase-frequency characteristic curve

Table 5. Parameters of equivalent circuit

Times	sample	R_s ($\Omega \cdot cm^2$)	Y_{01}(S-sec^n/cm^2)	n_1	R_f ($\Omega \cdot cm^2$)	Y_{02}(S-sec^n/cm^2)	n_2	R_{ct} ($\Omega \cdot cm^2$)
5days	T350	11.83	0.0001997	0.7955	764	0.002926	0.99	532
	T550	12.12	0.0001755	0.8015	985	0.001934	0.97	704
	T650	11.55	0.0001989	0.7953	1124	0.001216	0.89	852
10days	T350	12.23	0.0001411	0.8296	869	0.0005985	0.45	601
	T550	11.33	0.0000200	0.9721	983	0.0003581	0.69	1156
	T650	11.34	0.0000431	0.9588	1305	0.0002010	0.75	2044

Based on the above analysis for Table 4 and Table 5, R_s value changes a little, the average value is about 12, and the electrolyte resistance is almost the same, which explain each test system is in a state of relative stability. The value of Y_{02} are generally used to account for the deviation caused by the surface roughness due to corrosion, which will results in surface inhomogeneity on the microscopic level, such as porosity[18]. Lower the Y_{02} value is given for T650 steel than steels T350 and T550, it may caused by the increase tempering temperature. The polarization resistance from EIS can be expressed as $R_p = R_{ct} + R_f$, which has been widely used to account for the kinetics of electrochemical corrosion [19]. When the tempering temperature increases, R_p value increases. The R_p value of T650 is higher, which shows that corrosion resistance of T650 is much better than other steels. Compared with the Table 3, it is consistent with the polarization curves measurements.

3.6 Prediction model of corrosion rate

Based on the above analysis, we can see that T650 steel is better than the other steels about corrosion resistance. The corrosion rate is researched by grey system theory as follows. First, the test results of corrosion rate at different immersion time is given in Table 6.

Table 6. Corrosion rate of T650 steel at different immersion time

Time(Day)	1	2	3	4	5	6	7	8	9	10
corrosion rate(mm/a)	0.862	0.391	0.315	0.380	0.323	0.201	0.187	0.238	0.202	0.184

A first-order differential equation can be used to describe the behavior of the grey system. Accumulated generating operation(AGO) is an important feature of grey theory. By inverse accumulated generating operation(IAGO), the prediction can be converted back to the original datas[20]. A grey model GM(1,1) is shown as follows.

Suppose that the original series data is given.

$$x^{(0)} = \left(x^{(0)}(1), x^{(0)}(2), \cdots x^{(0)}(n)\right) \quad (3)$$

Then construct the accumulating generation operation of $x^{(0)}$ to form a new series of data.

$$x^{(1)}=\left(x^{(1)}(1),x^{(1)}(2),\cdots x^{(1)}(n)\right) \quad (4)$$

where $x^{(1)}(1)=x^{(0)}(1)$, $x^{(1)}(k)=\sum_{i=1}^{k}x^{(0)}(i),k=2,3,\cdots n$.

According to the grey system theory, the GM(1,1) mathematical model can be expressed by the following form.

$$\frac{\mathrm{d}x^{(1)}(t)}{\mathrm{d}t}=ax^{(1)}(t)+b \quad (5)$$

where a and b are unknown parameters.

The solution of differential equation (5) are given .

$$x^{(1)}(t)=\left(x^{(0)}(1)+\frac{b}{a}\right)e^{at}-\frac{b}{a} \quad (6)$$

Then we will demonstrate how to obtain the coefficients a and b .

First, we use difference quotient method to approximate the $\frac{\mathrm{d}x^{(1)}(t)}{\mathrm{d}t}$, have

$$\frac{\mathrm{d}x^{(1)}(t)}{\mathrm{d}t}=\lim_{\Delta t\to 0}\frac{x^{(1)}(k+\Delta t)-x^{(1)}(k)}{\Delta t} \quad (7)$$

where Δt is the time interval. We will take Δt as the unit time 1. The equation (7) is rewritten as

$$\frac{\mathrm{d}x^{(1)}(t)}{\mathrm{d}t}\approx x^{(1)}(k+1)-x^{(1)}(k) \quad (8)$$

Based on the principle of accumulative generate data, we have

$$x^{(1)}(k+1)-x^{(1)}(k)=x^{(0)}(k+1) \quad (9)$$

And substituting equations (8) and (9) into equation (5), we get the following form.

$$x^{(0)}(k+1)=ax^{(1)}(t)+b \qquad (k\le t\le k+1) \quad (10)$$

Using the value theorem of integrals, have

$$x^{(1)}(t)=\frac{1}{2}\left(x^{(1)}(k)+x^{(1)}(k+1)\right) \quad (k\le t\le k+1) \quad (11)$$

Then, we will substitute equation (11) into equation (10).

$$x^{(0)}(k+1)=\frac{1}{2}a\left(x^{(1)}(k)+x^{(1)}(k+1)\right)+b \quad (12)$$

Based on the above analysis, we will rewritte equation (12).

$$X_N\begin{bmatrix}a\\b\end{bmatrix}=Y_N \quad (13)$$

where

$$X_N=\begin{bmatrix}\frac{1}{2}\left(x^{(1)}(1)+x^{(1)}(2)\right) & 1\\ \frac{1}{2}\left(x^{(1)}(2)+x^{(1)}(3)\right) & 1\\ \vdots & \vdots\\ \frac{1}{2}\left(x^{(1)}(n-1)+x^{(1)}(n)\right) & 1\end{bmatrix},\quad Y_N=\begin{bmatrix}x^{(0)}(2)\\x^{(0)}(3)\\\vdots\\x^{(0)}(n)\end{bmatrix}.$$

To solve unknown coefficients a and b .

$$\begin{bmatrix}a\\b\end{bmatrix}=\left(X_N^TX_N\right)^{-1}\cdot X_N^T\cdot Y_N \quad (14)$$

The discrete prediction model is obtained.

$$\hat{x}^{(1)}(k+1)=\left(x^{(0)}(1)+\frac{b}{a}\right)e^{ak}-\frac{b}{a},\ \ k=1,2\ldots n \qquad (15)$$

$$\hat{x}^{(0)}(k+1)=\hat{x}^{(1)}(k+1)-\hat{x}^{(1)}(k) \qquad (16)$$

Finally, the established mathematical model is confirmed by residual error and variance. Specific steps are as follows.

Step 1: Calculating the average of original data $x^{(0)}$.

$$\overline{x}^{(0)}=\frac{1}{n}\sum_{i=1}^{n}x^{(0)}(i) \qquad (17)$$

Step 2: Calculating the mean variance S_1 of original data $x^{(0)}$.

$$S_1=\left(\frac{\sum_{i=1}^{n}\left[x^{(0)}(i)-\overline{x}^{(0)}\right]^2}{n-1}\right)^{1/2} \qquad (18)$$

Step 3: Calculating the residual error.

$$\Delta^{(0)}(i)=\left|x^{(0)}(i)-\hat{x}^{(0)}(i)\right|, i=1,2\ldots n \qquad (19)$$

Step 4: Calculating the average of residual error.

$$\overline{\Delta}^{(0)}=\frac{1}{n}\sum_{i=1}^{n}\Delta^{(0)}(i) \qquad (20)$$

Step 5: Calculating the mean variance S_2 of residual $\Delta^{(0)}$.

$$S_1=\left(\frac{\sum_{i=1}^{n}\left[\Delta^{(0)}(i)-\overline{\Delta}^{(0)}\right]^2}{n-1}\right)^{1/2} \qquad (21)$$

Step 6: Calculating variance ratio C.

$$C=\frac{S_2}{S_1} \qquad (22)$$

Step 7: Calculating small residual error probability P.

$$P=P\left\{\left|\Delta^{(0)}(i)-\overline{\Delta}^{(0)}\right|\right\}<0.6745S_1 \qquad (23)$$

Step 8: Judging the accuracy of prediction mode according to the standard. When the parameters $P>0.8$ and $C>0.5$, the established model is effective.

Finally, we will apply the grey model method into the prediction of corrosion rate for T650 steel, employing the experiment dates in table 6. The calculation steps for GM (1,1) model are described as follows. The original data is given for several days.

$$x^{(0)}=(0.862,0.391,0.315,0.380,0.323,0.201,0.187)$$

Then constructing the accumulation generation sequence

$$x^{(1)}=(0.862,1.253,1.568,1.948,2.271,2.472,2.703)$$

Next, we get the matrix X_N and Y_N.

$$X_N=\begin{bmatrix}1.0575 & 1\\ 1.4105 & 1\\ 1.7580 & 1\\ 2.1095 & 1\\ 2.3715 & 1\end{bmatrix},\ Y_N=\begin{bmatrix}0.391\\ 0.315\\ 0.380\\ 0.323\\ 0.201\end{bmatrix}.$$

We will substitute the above matrix data X_N and Y_N into equation (14). And the coefficients a and b are obtained by using the least square method,

$$\begin{bmatrix} a \\ b \end{bmatrix} = \begin{bmatrix} -0.1079 \\ 0.5099 \end{bmatrix}$$

The discrete response equation is given by solving the ordinary differential equation derivation method.

$$\hat{x}^{(1)}(k+1) = -3.8637e^{-0.1079k} + 4.7257$$

According to the above formula, we can get the accumulation generation sequence $\hat{x}^{(1)}$.

$$\hat{x}^{(1)} = (0.862, 1.257, 1.612, 1.930, 2.216, 2.473, 2.703)$$

Then forecast restore datas are obtained as follows.

$$\hat{x}^{(0)} = (0.862, 0.395, 0.355, 0.318, 0.286, 0.257, 0.230)$$

This can also predict the result after three days in Table 7.

Table 7. The forecast results of T650 steel at different immersion time

Time(Day)	1	2	3	4	5	6	7	8	9	10
corrosion rate(mm/a)	0.862	0.395	0.355	0.318	0.286	0.257	0.230	0.207	0.186	0.167

Finally, Based on the above ten sets of dates, according to the previous eight steps, we can work out $P = 1$ and $C = 0.09$ through programming method. This will prove that the established model are applicable to predict corrosion rate of low alloy steel.

The test dates are used to compare the forecast dates with GM(1,1) method in Figure 11.

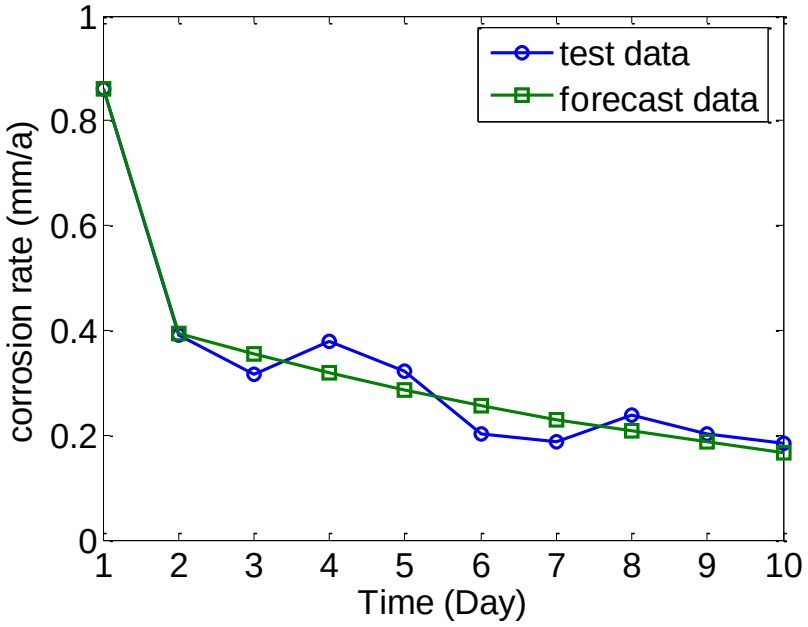

Figure 11. The comparison of corrosion rate for test and forecast data

From the Figure 11, we can see that the obtained mathematical model is feasible, which can be well used to forecast corrosion rate for the low alloy steel .

4. CONCLUSIONS

The microstructure and corrosion resistance of low alloy steel at different tempering temperature have been investigated. The conclusions are as follows:

1) The low alloy steel after tempering at 650^{o}C exhibits good corrosion resistance with a less weight loss, lower corrosion current density and bigger impedance modulus.

2) GM(1,1) model is employed to predict the corrosion rate of T650. The results indicated that the obtained mathematical model is feasible.

ACKNOWLEDGEMENTS
This work has been supported by the National Natural Science Foundation of China under Grant No.61403069, the Natural Science Foundation of Hebei Province (F2012501033, F2014501055, F2012501044) and the Technology Support Project of Northeastern University at Qinhuangdao (XNK201407).

References

1. F. Hayat, H. Yzun, *J. Iron. Steel. Res. Int.*, 18(2011)65.
2. J. Liu, H. Yu, Z. Tao, *Mater. Sci. Eng.A*, 619 (2014)212.
3. H. S. Ren, X. J. Tian, H. M. Wang, *Mater. Sci. Eng.A*, 614 (2014) 207.
4. T. V. Shibaeva, V. K. Laurinavichyute, G. A. Tsirlina, *Corros.Sci*, 80(2014) 299.
5. X. M. Yu, Y. L. Huang, W. J. Qu, *Int.J.Electrochem.Sci.*, 9(2014)3760.
6. J. Y. Park, Y. S. Park, *Mater. Sci. Eng. A*, 449(2007) 1131.
7. J. Wang. Z. Y. Wang, W. Ke, *Mater. Chem. Phys.*, 124(2010)952.
8. Y. Zou, J. Wang, Y. Y. Zheng, *Corros.Sci.*, 53(2011)208.
9. X. L. Zhou, L. Nie, X. Z. Hua, Z. Y. Liu, X. Cui, *J. Chin, Soc. Corros. Prot.*, 32(2012) 423.
10. S. Marcelin, N. Pébère, S. Régnier, *Electrochim. Acta.*, 87(2013) 32.
11. S. W. Kim, H. W. Lee, *Int.J.Electrochem.Sci.*,9(2014) 4709.
12. M. A. Lucio, J. G. Gonzalez, M. Casales, *Corros.Sci.*, 51(2009)2380.
13. S. B. Kargar, M. H. Moayed, A. Babakhani, *Corros.Sci.*, 53(2011)135.
14. R. G. Li, W. J. He, *Phys. Procedia*, 33(2012)162.
15. F.Y. Ma, W. H. Wang, *Mater. Lett.*, 61(2007)998.
16. F. L. Sun, X. G. Li, F. Zhang, *Acta. Metall. Sin.*, 26(2013)257.
17. Y. Zou, J. Wang, Y.Y. Zheng, *Corros.Sci.*, 53(2011)208.
18. R. Wang, S. J. Lou, M. Liu, Y. N. Xue, *Corros.Sci.*, 85(2014) 270.
19. A. V. C. Sobral, W. Ristow, D. S. Azambuja, I. Costa, C. V. Franco, *Corros.Sci.*, 43(2001) 1019.
20. X. M. Shen, Z. N. Lu, *AASRI Procedia*, 7(2014) 81.